

Peak effects and the solid vortex phase of a T^* -phase $\text{SmLa}_{0.8}\text{Sr}_{0.2}\text{CuO}_{4-\delta}$ single crystal

I. M. Sutjahja and A. A. Nugroho

*Van der Waals–Zeeman Instituut, Universiteit van Amsterdam, Valckenierstraat 65, 1018 XE, Amsterdam, The Netherlands
and Jurusan Fisika, Institut Teknologi Bandung, Jl. Ganesha 10, Bandung 40132, Indonesia*

M. O. Tjia

Jurusan Fisika, Institut Teknologi Bandung, Jl. Ganesha 10, Bandung 40132, Indonesia

A. A. Menovsky and J. J. M. Franse

Van der Waals–Zeeman Instituut, Universiteit van Amsterdam, Valckenierstraat 65, 1018 XE, Amsterdam, The Netherlands

(Received 27 March 2001; revised manuscript received 11 June 2001; published 28 August 2001)

The isothermal magnetization curves obtained from a superconducting T^* -phase $\text{SmLa}_{0.8}\text{Sr}_{0.2}\text{CuO}_{4-\delta}$ single crystal have demonstrated the existence of distinct peak effect in a large temperature range, persisting up to the vicinity of the superconducting critical temperature ($T_c^{\text{on}} \approx 24$ K). The magnetization curves also exhibit the remarkable feature of zero-field peaking and its enhancement at lower temperature. Analysis of the associated vortex phase diagram further establishes the role of geometrical barrier in the retardation of vortex penetration at high temperature and that of surface barrier at lower temperature. The temperature dependence of the second peak field is also found to conform with existing models at the appropriate temperature regimes. Additionally, the irreversibility line shows a sign reversal of its slope at a field position around H_{2D} indicating two-dimensional melting at higher field. Nevertheless, the temperature dependent behavior of the second peak onset field is at variance with other published results and defies explanation on the basis of existing theoretical models.

DOI: 10.1103/PhysRevB.64.134502

PACS number(s): 74.72.Dn, 74.25.Dw, 74.25.Ha

I. INTRODUCTION

The magnetic phase diagram of a vortex system in a cuprate superconductor is known to exhibit a number of intriguing features which have become topics of extensive theoretical and experimental researches.¹ These new features are generally understood to have their origins in the unusual intrinsic properties of the materials. Aside from the relatively high critical temperature, the most remarkable characteristics of the cuprate superconductors are the high degree of anisotropy associated with the layered structure, and the thermal fluctuation effects arises mainly from the short coherence length. As a consequence, the rich and complicated vortex phase diagram must be analyzed on the basis of interplay between three basic energy scales, the vortex elastic energy (E_{elastic}), thermal fluctuation energy (E_{thermal}), and pinning energy (E_{pinning}).¹

One of the long standing research issues regarding the vortex ensemble in the cuprate superconductor is the physical mechanism underlying the anomalous increase of magnetization with increasing magnetic field applied parallel to the c axis above the lower critical field H_{c1} , the so called peak-effect or fishtail effect. This phenomenon has been observed in a relatively clean and high quality single crystals of $\text{YBa}_2\text{Cu}_3\text{O}_{7-\delta}$ (YBCO),²⁻⁷ $\text{Nd}_{1.85}\text{Ce}_{0.15}\text{CuO}_{4-\delta}$ (NCCO),⁸⁻¹¹ $(\text{La}_{1-x}\text{Sr}_x)_2\text{CuO}_{4-\delta}$ (LSCO),¹²⁻¹⁴ $\text{Bi}_2\text{Sr}_2\text{CaCu}_2\text{O}_8$ (BSCCO),¹⁵⁻²¹ $(\text{Bi,Pb})_2\text{Sr}_2\text{CaCu}_2\text{O}_8$ (BPSCCO),²²⁻²⁴ Tl-based compounds,^{15,25-28} and $\text{HgBa}_2\text{CuO}_4$ (HBCO).²⁹ The same effect has also been reported for the low-temperature superconductor (LTS) of 2H-NbSe_2 ,³⁰ intermetallic compound of CeRu_2 ,³¹ as well as organic materials such as κ -(BEDT-TTF)₂Cu(NCS)₂ (Refs.

32,33) and the noncuprate oxide system of $(\text{Ba,K})\text{BiO}_3$.³⁴ The peak effect was generally found to disappear above some characteristic temperature well below T_c for the highly anisotropic high- T_c systems such as BSCCO, while it was found to persist up to a temperature approaching T_c in the less anisotropic high T_c system such as YBCO and the low- T_c systems such as the 214 cuprate superconductors. This effect has been studied extensively, and attributed to mechanism varying from collective pinning,³⁵ surface barriers,^{8,15,16} and lattice matching effect between the vortex and defect structures.¹⁸ Other mechanisms proposed in the literature include the three-dimensional–two-dimensional (3D-2D) crossover,¹⁹ crossover between elastic and plastic states,³ crossover between quasilattice vortex glass and disorder vortex glass,³⁶⁻³⁸ and thermal-disorder induced interlayer decoupling transition of the vortex pancake.^{22,39} In spite of these wide ranging results, a unified understanding of the phenomenon is still lacking.

The 214 system of the cuprate superconductors with its relatively low T_c is known to exist in three different phases, namely, the T phase in the family of $\text{La}_{2-x}\text{M}_x\text{CuO}_{4-\delta}$ ($M = \text{Ba, Sr, Ca}$), the T' phase in the family of $\text{R}_{2-x}\text{A}_x\text{CuO}_{4-\delta}$ ($R = \text{Pr, Nd, Sm, Eu, Tm}$; $A = \text{Ce, Th}$) and the T^* phase in the family of $(\text{M}_{1-x-y}\text{M}'_x\text{Sr}_y)_2\text{CuO}_{4-\delta}$ ($M = \text{La, Nd, Pr}$; $M' = \text{Ce, Sm, Eu, Gd, Tb, Dy, Ho, and Y}$). This system has so far stood out as the only known cuprate system which can accommodate different types of charge carrier doping, i.e., hole doping in the T and T^* phases and electron doping in the T' phase. With its moderately large ξ_{ab} compared to other high- T_c cuprate superconductors, this system offers a unique advantage of experimental accessibility of the whole

range of magnetic phase up to its normal state. Given its additional advantage of having a single layer of CuO_2 , this system serves as an ideal model for the much needed study of structure-property correlation.

Up till now, most research works on this 214 system have been devoted to the T and T' phases, presumably due to greater obstacle in obtaining a good quality single crystal of the T^* phase. On the other hand, the study of the T^* phase is likely to provide additional insight to the understanding of the peak effect and other related properties due to its unique structure embedding two different phases in one system. Being a hybrid of T phase $[(\text{La}_{1-x}\text{Sr}_x)_2\text{CuO}_{4-\delta}]$ and T' phase $(\text{Sm}_2\text{CuO}_{4-\delta})$, this system is expected to exhibit interesting new features in its vortex phase structure and the associated transitional behaviors. This will in turn provide additional experimental data for the study of structure-property correlation. With this hope in mind, we have undertaken the task of growing the single crystal of T^* phase $\text{SmLa}_{1-x}\text{Sr}_x\text{CuO}_{4-\delta}$ for the study of its vortex behavior. In this paper, we report the results of magnetic measurements of a $\text{SmLa}_{0.8}\text{Sr}_{0.2}\text{CuO}_{4-\delta}$ single crystal, demonstrating the fishtail effect in a large temperature range below T_c . It will be shown that most of these magnetization data do conform with the existing models, while others, such as the onset field of the second peak effect, are clearly in need of further theoretical and experimental studies.

EXPERIMENTS

Single crystals of $\text{SmLa}_{0.8}\text{Sr}_{0.2}\text{CuO}_{4-\delta}$ were grown by the traveling solvent floating zone (TSFZ) method using a four-mirror furnace from Crystal System, Inc. A crystal with dimensions of $\sim 2.0 \times 2.0 \times 0.9 \text{ mm}^3$ and a mass of $\sim 23 \text{ mg}$ was obtained by cleaving the as-cut crystal in air along the ab plane. The superconductivity of the crystal was attained by annealing the as grown crystal in 200 bar oxygen at 600°C for 7 days, followed by another heat treatment at 300°C for 3 days before being cooled slowly to room temperature at a rate of 25°C/hr . The onset of the critical transition temperature after this oxidation process is found to be $T_c^{\text{on}} \approx 24 \text{ K}$ with $\Delta T_c \approx 3 \text{ K}$ as depicted by the $M-T$ curve in Fig. 1. Details on this crystal growth process, its oxidation effect and structural characterization of the crystal will be published elsewhere.⁴⁰

A series of isothermal magnetic measurements were performed with the external magnetic field H applied parallel to the c axis of the crystal using a commercial Quantum Design MPMS-5 magnetometer. To ensure field homogeneity during the measurement, a scan length of 4 cm was used, and each measurement was started after cooling the sample in zero field (ZFC mode) to the predetermined temperature.

RESULTS OF MEASUREMENT

The data presented in Figs. 2–6 are the results of isothermal magnetization loop measurement carried out over the temperature range from 2 to 20 K, at a temperature interval of 1 K. The $M(H)_T$ curves obtained clearly separate into two groups associated, respectively, with the temperature regions

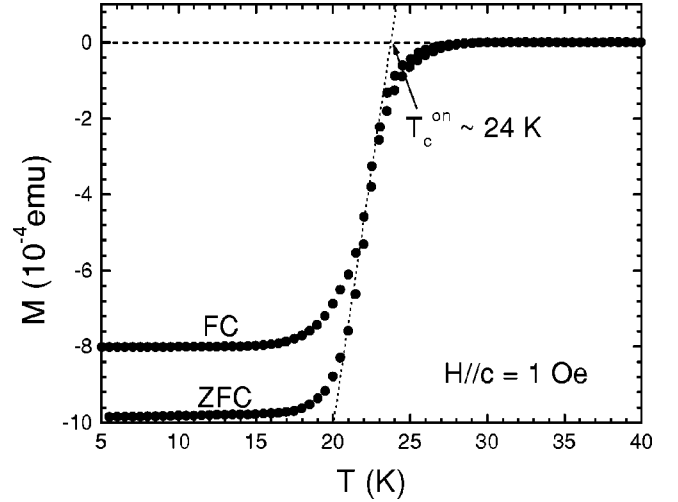


FIG. 1. Temperature dependence of magnetization of $\text{SmLa}_{0.8}\text{Sr}_{0.2}\text{CuO}_{4-\delta}$ single crystal after oxygen annealing and slow cooling as described in the text, showing the screening (ZFC-mode) and Meissner (FC-mode) effects.

of $9 \leq T \leq 20 \text{ K}$ (Figs. 2–4) and $2 \leq T \leq 8 \text{ K}$ (Figs. 5,6). In the higher temperature region, a distinct second peak is observed on each of the magnetization curves with varying position and magnitude. The position of this second peak H_{SP} together with those of the onsets of field penetration H_p , the onset of the second peak effect H_{on} as well as the irreversible field H_{irr} are indicated in Fig. 2 for easy identification. The penetration field H_p is determined as the first minimum of magnetization on the curve, the onset field of peak effect H_{on} as the first maximum and the second peak field H_{SP} as the second minimum on the curve. The irreversibility field H_{irr} is determined from the $M(H)_T$ curves as the point where the difference between the values of the magnetization for in-

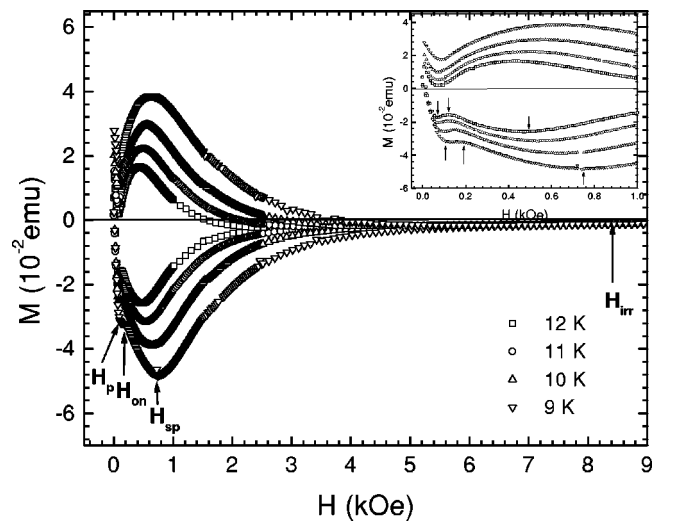


FIG. 2. Isothermal magnetic-hysteresis loops of a $\text{SmLa}_{0.8}\text{Sr}_{0.2}\text{CuO}_{4-\delta}$ single crystal measured at various temperatures between 9 and 12 K. The penetration field H_p , the onset field of the second peak H_{on} , the second peak field H_{SP} , and the irreversible field H_{irr} are indicated by the arrowheads.

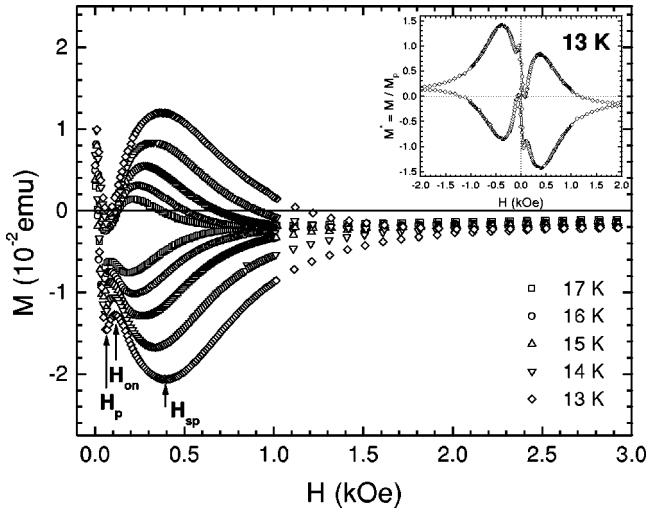


FIG. 3. Isothermal magnetic-hysteresis loops of a $\text{SmLa}_{0.8}\text{Sr}_{0.2}\text{CuO}_{4-\delta}$ single crystal measured at various temperatures between 13 and 17 K. The penetration field H_p , the onset field of the second peak H_{on} , and the second peak field H_{SP} are indicated by the arrowheads. The inset shows the peak effect at zero field in the hysteresis loop at 13 K, normalized by M value at the corresponding H_p .

creasing and decreasing field begins to deviate from zero to within the accuracy of the experiment ($\pm 5 \times 10^{-6}$ emu). We note that a near perfect mirror symmetry between the ascending and descending branches of the hysteresis loop clearly features on all the curves in this temperature region. As we enter the lower temperature region ($T < 9$ K), the peak effect on the ascending branch becomes weaker with decreasing temperature, while the mirror symmetry mentioned earlier fades away concurrently. In this temperature range, the pen-

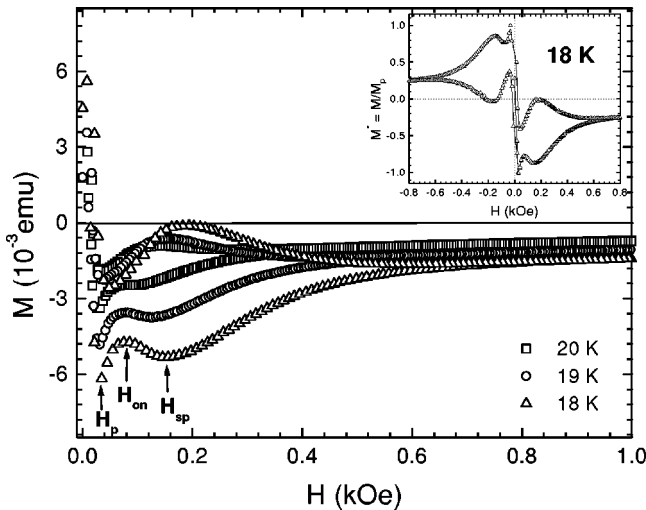


FIG. 4. Isothermal magnetic-hysteresis loops of a $\text{SmLa}_{0.8}\text{Sr}_{0.2}\text{CuO}_{4-\delta}$ single crystal measured at various temperatures between 18 and 20 K. The penetration field H_p , the onset field of the second peak H_{on} , and the second peak field H_{SP} are indicated by the arrowheads. The inset shows the peak effect at zero field in the hysteresis loop at 18 K, normalized by M value at the corresponding H_p .

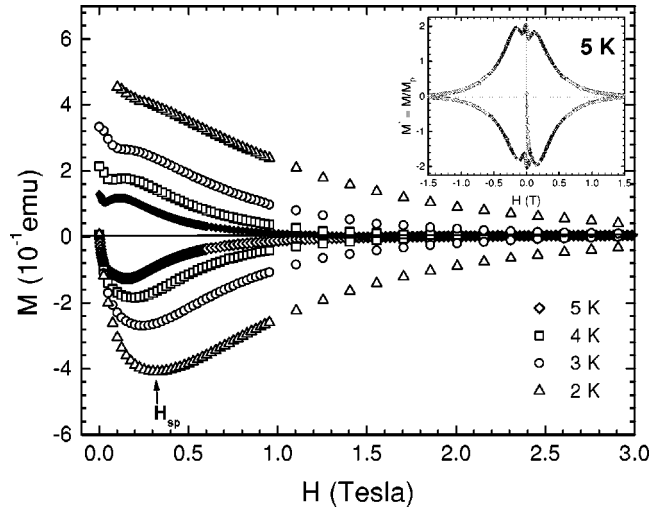


FIG. 5. Isothermal magnetic-hysteresis loops of a $\text{SmLa}_{0.8}\text{Sr}_{0.2}\text{CuO}_{4-\delta}$ single crystal measured at various temperatures between 2 and 5 K. The second peak field H_{SP} is indicated by the arrowhead. The inset shows the peak effect at zero field in the hysteresis loop at 5 K, normalized by M value at the corresponding H_p .

etration field H_p appears more similar to a kink instead of a peak, similar to the result reported for $\text{Tl}_2\text{Ba}_2\text{CuO}_6$ single crystal.²⁶ A closer look at the field above H_p reveals a curvature change located slightly above H_p . This is identified as the onset of a second peak field, determined as the point of inflection satisfying $d^2M/dH^2=0$ as illustrated by the inset in Fig. 6.

In order to facilitate the following analysis and discussion of the experimental results, the characteristic fields (H_p , H_{on} , H_{SP} , and H_{irr}) on each magnetization curve have been

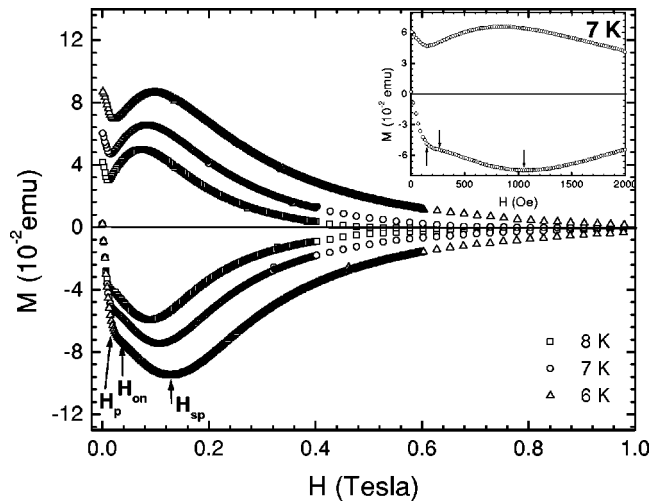


FIG. 6. Isothermal magnetic-hysteresis loops of a $\text{SmLa}_{0.8}\text{Sr}_{0.2}\text{CuO}_{4-\delta}$ single crystal measured at various temperatures between 6 and 8 K. The penetration field H_p , the onset field of the second peak H_{on} , and the second peak field H_{SP} are indicated by the arrowheads. The inset shows the low-field part of the curve at 7 K, indicating the characteristic fields H_p , H_{on} , and H_{SP} on the curve (see text for details).

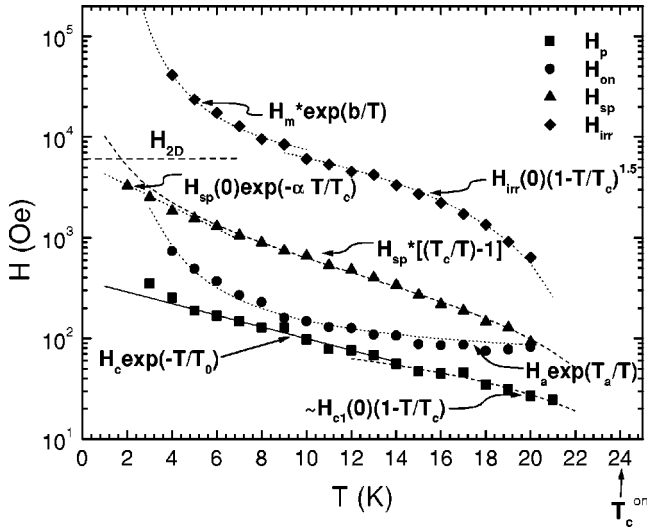


FIG. 7. The magnetic phase diagram of a $\text{SmLa}_{0.8}\text{Sr}_{0.2}\text{CuO}_{4-\delta}$ single crystal, showing the temperature dependencies of penetration field H_p , onset field H_{on} , second peak field H_{sp} and the irreversible field H_{irr} . The theoretical fits of these transition lines are indicated by either the dotted, dashed, and solid lines for easy distinction. See text for discussions.

converted point by point for each temperature into the H - T phase diagram. The result is given in Fig. 7, which indicates the separation of the entire solid phase area into a number of distinct regions bounded by the associated "phase lines." These experimental curves are the objects of our analysis and discussion on the basis of existing models.

ANALYSIS AND DISCUSSION

We note that the data of penetration field in Fig. 7 show a general trend of increasing H_p with decreasing temperature. It is well known that this general temperature dependent behavior of H_p has been theoretically predicted by the surface barrier model⁴¹ as well as the geometrical barrier model⁴² and experimentally verified in several systems^{10,11,15,29,43} and different temperature ranges.^{8,20,21,44} The surface barrier model predicts for a strongly layered system a functional relation of the form $H_p(T) \approx H_c \exp(-T/T_0)$ where T_0 is a constant. For a less anisotropic (quasi-3D) system, this model yields the approximate expression $H_p(T) \propto (T_c - T)^{3/2}/T$ for $H_p < H_c$. On the other hand, the geometrical barrier model leads to a penetration field H_p having the temperature dependence given by $H_p(T) = H_p(0)(1 - T/T_c)$, which is expected to be dominant at elevated temperature. The results of best fit to our data on the basis of these models are depicted in the figure. It is seen that the data for $T \geq 14$ K are closely fitted by the geometrical barrier model with $H_p(0) = 116$ Oe and $T_c = 26.3$ K which begins to deviate from the data below 14 K. This result confirms previous observations on $\text{Nd}_{1.85}\text{Ce}_{0.15}\text{CuO}_{4-\delta}$ (Ref. 8) and $\text{Bi}_2\text{Sr}_2\text{CaCu}_2\text{O}_8$ (Refs. 20,21,42) crystals in the elevated temperature regime.

In the lower-temperature regime where the bulk pinning and surface barrier are supposed to be important we have

found a good fit with the exponential function with $H_c = 377$ Oe and $T_0 = 7.5$ K, as observed previously on $\text{Bi}_2\text{Sr}_2\text{CaCu}_2\text{O}_8$,^{15,20,21} $\text{Tl}_2\text{Ba}_2\text{CaCu}_2\text{O}_8$,^{15,43} $\text{Nd}_{2-x}\text{Ce}_x\text{CuO}_{4-\delta}$,^{8,10,11} and $\text{HgBa}_2\text{CuO}_4$ (Ref. 29) crystals, but failed to fit the quasi 3D relation in contrast to previous observation reported on $\text{Bi}_2\text{Sr}_2\text{CaCu}_2\text{O}_8$ by Nideröst *et al.*⁴⁴ It must be noted, however, that perceptible deviation from the exponential function does occur at the lower end of the temperature range. This may well be attributed to the significant bulk pinning at low temperature below 5 K explaining the need of a higher external field for its effective penetration into the sample. It is not clear whether this deviation mainly manifest the effect of bulk pinning or may have some contribution from the measurement conducted at a faster pace below 5 K as pointed out in an earlier report.⁴⁴

Further, let us turn our attention to the insets of Figs. 3, 4, and 5, where the descending magnetization curves exhibit sharp peaks at a negative field close to zero. The "zero-field" peaks observed in magnetization curves of high-temperature superconductors⁴⁵ were theoretically explained by Zeldov *et al.* as an important effect of geometrical barrier in the sample, which becomes significantly enhanced in the presence of Bean Livingston surface barrier.⁴² Our data of the zero-field peak as displayed in those insets in terms of its normalized value with respect to magnetization at the corresponding H_p also show its enhancement at lower temperature where the surface barrier is expected to become operative. These observations constitute a clear support for the theoretical description of Zeldov *et al.*⁴²

We turn next to the H_{on} curve located slightly above H_p . As mentioned earlier, this curve marks the onset of the fish-tail effect which is commonly associated with a transition between two solid phases. A recent model proposed by Giller *et al.*⁹ describes the effect as a disorder-induced transition, taking place at a field determined by the competition between the vortex elastic energy $E_{elastic}$ and the pinning energy $E_{pinning}$. The elastic interaction at low field governs the structure of the vortex solid leading to the formation of a quasi-ordered lattice (Bragg glass), while disorder becomes dominant at high field where the interaction between the vortices and the pinning centers results in an entangled solid (vortex glass).^{36-38,9} According to this model, the characteristic cross over field H_{on} has a temperature dependence of the form $H_{on}(T) = H_{on}(0)[1 - (T/T_c)^4]^{3/2}$. We have found that this functional relationship, showing an opposite curvature, can hardly fit our data, as was reported previously for the systems of $\text{Nd}_{1.85}\text{Ce}_{0.15}\text{CuO}_{4-\delta}$ (Ref. 11) and $(\text{Bi,Pb})_2\text{Sr}_2\text{CaCu}_2\text{O}_{8+\delta}$.²⁴ On the other hand, our data in the temperature range of 4–20 K are much better fitted by an exponential function of $H_{on}(T) = H_a \exp(T_a/T)$, with $H_a = 50$ Oe and $T_a = 11$ K. It is worth noting that this curve extrapolates at both ends of the temperature range toward the H_{sp} field at temperatures where the peak effect is supposed to disappear completely. We recall that this is precisely the phenomenon depicted in Fig. 5. This exponential T -dependent behavior is nevertheless in dire contrast to the exponential dependence of $H_{on}(T) = H_0 \exp(-T/T_0)$ reported for $\text{Tl}_2\text{Ba}_2\text{CuO}_6$ (Ref. 27) and $\text{HgBa}_2\text{CuO}_4$ (Ref. 29) sys-

tems. To the best of our knowledge, explanations of these different results are not available from the existing theoretical models.

The data of second peak field $H_{SP}(T)$ is examined on the basis of thermal decoupling theory.^{22,39,46–49} This theory predicts the suppression of superconducting long-range order in the direction of the applied field due to thermal fluctuation of the pancake vortices, leading to the decoupling of the pancake vortex layers. In the $(\text{Sm,La,Sr})_2\text{CuO}_4$ crystal, the moderate value of anisotropy parameter γ satisfies the condition $\xi_{ab} \ll \gamma s \ll \lambda_{ab}$, where ξ_{ab} and λ_{ab} are the in-plane coherence length and penetration depth, respectively, while s is the CuO_2 interlayer distance. Assuming a mean-field temperature dependence of $\lambda_{ab}^2(T) = \lambda_{ab}^2(0)/(1 - T/T_c)$, the decoupling field H_d is then given by^{46,47} $H_d(T) = \Phi_0^3/[16\pi^3 e k_B \mu_0 s \gamma^2 T \lambda_{ab}^2(T)]$, with Φ_0 denoting the flux quantum (2.07×10^{-15} Wb), k_B the Boltzmann constant (1.38×10^{-23} J/K), and μ_0 the permeability of free space ($4\pi \times 10^{-7}$ H/m). Based on this model the second peak field is supposed to have a temperature dependence of $H_{SP}(T) = H_{SP}^*[(T_c/T) - 1]$ with $H_{SP}^* = \Phi_0^3/[16\pi^3 e k_B \mu_0 s \gamma^2 T_c \lambda_{ab}^2(0)]$. This function can be nicely fitted to the data points with the value of $H_{SP}^* = 430$ Oe and $T_c = 24.6$ K. This result indicates that the second peak effect, weakening at high temperatures in the T^* phase of $\text{SmLa}_{0.8}\text{Sr}_{0.2}\text{CuO}_{4-\delta}$, has its origin in the thermal disorder-induced interlayer decoupling. A similar analysis was reported on an overdoped $(\text{Bi,Pb})_2\text{Sr}_2\text{CaCu}_2\text{O}_{8+\delta}$ (Ref. 22) and qualitatively on $\text{Tl}_2\text{Ba}_2\text{CuO}_6$ (Ref. 27) single crystals. Substituting the parameter s in the theoretical expression of H_{SP}^* by the value $s = c \approx 12.60$ Å obtained from the refinement analysis of XRD pattern,⁴⁰ we arrive at the zero temperature in-plane penetration depth of $\lambda_{ab}(0) \approx 3634$ Å. This value is very close to that of T phase $\text{La}_{1.875}\text{Sr}_{0.125}\text{CuO}_{4-\delta}$.⁵⁰ It must be stressed nevertheless, that the lower-temperature part of the second peak data ($T \leq 5$ K) is better described by an exponential function of $H_{SP}(T) = 5500 \exp(-T/4)$ in conformity with the expression $H_{SP}(T) = H_{SP}(0) \exp(-\alpha T/T_c)$ as adopted in the previous analysis of Tl-based single crystal^{26,28} and $(\text{Bi,Pb})_2\text{Sr}_2\text{CaCu}_2\text{O}_{8+\delta}$ single crystal.²⁴ This different behavior in the lower-temperature region ($T \leq 5$ K) is most likely a manifestation of a different pinning mechanism as a consequence of diminishing role of thermal energy.

The temperature dependence of the irreversibility line $H_{irr}(T)$ as depicted in Fig. 7 shows a curvature reversal around 10 K, from negative curvature at higher temperature-low field region to positive curvature at lower temperature-high field region. The data in the higher temperature region ($10 \leq T \leq 20$ K) displays an excellent fit to the theoretical curve given by $H_{irr}(T) = H_{irr}(0)(1 - T/T_c)^{3/2}$ with $H_{irr}(0) = 15$ kOe and $T_c = 22.5$ K. This temperature dependency is supposed to indicate the dominance of thermal effect as predicted by the giant flux creep models of Yeshurun⁵¹ and Tinkham.⁵² In the lower temperature region ($T < 10$ K), the H_{irr} curve exhibiting positive curvature is very well fitted by an exponential dependence of the form $H_{irr}(T) = H_m \exp(b/T)$, with $H_m = 2500$ Oe and $b = 11$ K. This behavior has been suggested in the quasi 2D Josephson coupled

layer-superconductor (JCLS) model with moderate anisotropy.⁵³ It is tempting at this point to consider the empirical formula proposed by Kitazawa *et al.*,⁵⁴ which relates the anisotropy parameter γ to the measured irreversibility field $H_{irr}(T)$, namely, $H_{irr}(T) = 33\,400/\gamma^2(1 - T/T_c)^m$. This empirical equation is based on the consideration that the cuprate HTSC compound can be viewed universally as a system of alternating insulating/blocking and superconducting layers.⁵⁵ In such a system, the associated anisotropy is expected to control various electromagnetic phenomena including flux pinning strength. Equating the multiplicative factor in this equation with the $H_{irr}(0)$, obtained above from the constant factor of the irreversibility line in the higher-temperature region, yields the value of $\gamma \approx 47$ which lies between those of $(\text{La,Sr})_2\text{CuO}_{4-\delta}$ system ($\gamma = 14\text{--}63$) (Ref. 54) and $(\text{Nd,Ce})_2\text{CuO}_{4-\delta}$ system ($\gamma = 30\text{--}100$).⁵⁶

A rough estimation of dimensional crossover field (3D-quasi 2D crossover) H_{2D} following the approximate formula⁴⁷ $H_{2D} \approx \Phi_0/\lambda_J^2$ with $\lambda_J = \gamma s$ and $\gamma \approx 47$ yields the value $H_{2D} \approx 6000$ Oe. Looking at the H - T phase diagram, this H_{2D} value is located approximately at the field where the H_{irr} curve undergoes sign reversal in its slope, marking the onset of weakening interlayer coupling and indicating 2D melting at higher field. This view is consistent with steep rise of $H_{irr}(T)$ for $H > H_{2D}$, approaching the well known theoretical prediction of field independent melting line $H_m(T)$ for the strongly layered 2D system.⁵³ Although the dimensional crossover H_{2D} given above is strictly valid only in the low-temperature region far away from T_c , the near coincidence between H_{2D} and the curvature reversal of $H_{irr}(T)$ is nevertheless an interesting point to note in the context explained above.

The estimation of the out-of-plane penetration depth at zero temperature $\lambda_c(0)$ based on the estimated anisotropy parameter γ and zero temperature in-plane penetration depth $\lambda_{ab}(0)$ according to the general formula $\gamma = \lambda_c/\lambda_{ab}$ yields $\lambda_c(0) \approx 17.08 \mu\text{m}$. This value is smaller than the one observed from optical measurement obtained from the same batch of crystals under different oxygen annealing treatment, namely $\lambda_c(3\text{K}) \approx 45 \mu\text{m}$.⁵⁷ We are inclined to attribute this discrepancy to different carrier doping levels in these two crystals, in congruence with different anisotropy parameters and different critical temperatures. The crystal used for optical measurement is known as a strongly underdoped sample ($T_c \approx 16$ K), while our sample is approximately in the optimal doping state ($T_c^{\text{on}} \approx 24$ K).

CONCLUSION

We have demonstrated from the isothermal magnetization data of $\text{SmLa}_{0.8}\text{Sr}_{0.2}\text{CuO}_{4-\delta}$ single crystal with $T_c^{\text{on}} \approx 24$ K that this system exhibits the well known peak effect in a large temperature range, extending from 2 to 20 K. Additionally, the magnetization data also reveal remarkable zero-field peak throughout most of the same temperature range, with perceptible enhancement at lower temperatures. Analysis of the magnetic phase diagram derived from these data on the basis of an existing models clearly indicates the role of geometrical barrier in the retardation of vortex penetration at

elevated temperature range, and that of surface barrier at lower temperature. We have also found that most of the data in various temperature and field regions can be well described with the existing theoretical models. In particular, a slope change of the irreversibility line at the field position around H_{2D} confirms the 2D melting characteristics at $H > H_{2D}$. One exception is the temperature dependent behavior of the second peak onset field $H_{on}(T)$ which appears to defy explanation by any model known to the authors. Further, estimations of the anisotropy parameter and penetration depth at zero temperature have also been made, yielding a

value between those of T and T' 214 systems, and thereby provide further indication of the different features occurring in this T^* phase compared to the other 214 compounds.

ACKNOWLEDGMENTS

We are grateful to FOM-ALMOS for the use of sample preparation and characterization facilities. This work was carried out under the cooperation of the Van der Waals–Zeeman Institute and Jurusan Fisika ITB supported by KNAW under Project No. 95-BTM-33.

- ¹G. Blatter, M. V. Feigel'man, V. B. Geshkenbein, A. I. Larkin, and V. M. Vinokur, *Rev. Mod. Phys.* **66**, 1125 (1994).
- ²M. Daeumling, J. M. Seuntjens, and D. C. Larbalestier, *Nature (London)* **346**, 332 (1990).
- ³Y. Abulafia, A. Shaulov, Y. Wolfus, R. Prozorov, L. Burlachkov, Y. Yeshurun, D. Majer, E. Zeldov, H. Wühl, V. B. Geshkenbein, and V. M. Vinokur, *Phys. Rev. Lett.* **77**, 1596 (1996).
- ⁴T. Nishizaki, T. Naito, and N. Kobayashi, *Phys. Rev. B* **58**, 11 169 (1998).
- ⁵S. Salem-Sugui, L. Ghivelder, M. Friesen, K. Moloni, B. Veal, and P. Paulikas, *Phys. Rev. B* **60**, 102 (1999).
- ⁶D. Giller, A. Shaulov, Y. Yeshurun, and J. Giapintzakis, *Phys. Rev. B* **60**, 106 (1999).
- ⁷M. Pissas, E. Moraitakis, G. Kallias, and A. Bondarenko, *Phys. Rev. B* **62**, 1446 (2000).
- ⁸F. Zuo, S. Khizroev, X. Jiang, J. L. Peng, and R. L. Greene, *Phys. Rev. B* **49**, 12 326 (1994).
- ⁹D. Giller, A. Shaulov, R. Prozorov, Y. Abulafia, Y. Wolfus, L. Burlachkov, Y. Yeshurun, E. Zeldov, V. M. Vinokur, J. L. Peng, and R. L. Greene, *Phys. Rev. Lett.* **79**, 2542 (1997).
- ¹⁰M. C. de Andrade, N. R. Dilley, F. Ruess, and M. B. Maple, *Phys. Rev. B* **57**, R708 (1998).
- ¹¹A. A. Nugroho, I. M. Sutjahja, M. O. Tjia, A. A. Menovsky, F. R. de Boer, and J. J. M. Franse, *Phys. Rev. B* **60**, 15 379 (1999).
- ¹²T. Kimura, K. Kishio, T. Kobayashi, Y. Nakamura, N. Motohira, K. Kitazawa, and K. Yamafuji, *Physica C* **192**, 247 (1992).
- ¹³M. Okuya, T. Sasagawa, T. Kimura, J. Shimoyama, K. Kitazawa, and K. Kishio, *Physica C* **271**, 265 (1996).
- ¹⁴Y. Kodama, K. Oka, Y. Yamaguchi, Y. Nishihara, and K. Fujimura, *Phys. Rev. B* **56**, 6265 (1997).
- ¹⁵V. N. Kopylov, A. E. Koshelev, I. F. Schegolev, and T. G. Togonidze, *Physica C* **170**, 291 (1990).
- ¹⁶N. Chikumoto, M. Konczykowski, N. Motohira, and A. P. Malozemoff, *Phys. Rev. Lett.* **69**, 1260 (1992).
- ¹⁷K. Kadowaki and T. Mochiku, *Physica C* **195**, 127 (1992).
- ¹⁸G. Yang, P. Shang, S. D. Sutton, I. P. Jones, J. S. Abell, and C. E. Gough, *Phys. Rev. B* **48**, 4054 (1993).
- ¹⁹T. Tamegai, Y. Iye, I. Ogura, and K. Kishio, *Physica C* **213**, 33 (1993).
- ²⁰E. Zeldov, D. Majer, M. Konczykowski, A. I. Larkin, V. M. Vinokur, V. B. Geshkenbein, N. Chikumoto, and H. Shtrikman, *Europhys. Lett.* **30**, 367 (1995).
- ²¹C. D. Dewhurst, D. A. Cardwell, A. M. Campbell, R. A. Doyle, G. Balakrishnan, and D. McK. Paul, *Phys. Rev. B* **53**, 14 594 (1996).
- ²²Y. P. Sun, Y. Y. Hsu, B. N. Lin, H. M. Luo, and H. C. Ku, *Phys. Rev. B* **61**, 11 301 (2000).
- ²³M. Baziljevich, D. Giller, M. McElfresh, Y. Abulafia, Y. Radzyner, J. Schneck, T. H. Johansen, and Y. Yeshurun, *Phys. Rev. B* **62**, 4058 (2000).
- ²⁴D. Darminto, M. O. Tjia, T. Motohashi, H. Kobayashi, Y. Nakayama, J. Shimoyama, and K. Kishio, *Phys. Rev. B* **62**, 6649 (2000).
- ²⁵V. Hardy, A. Wahl, A. Ruyter, A. Maignan, C. Martin, L. Coudrier, J. Provost, and Ch. Simon, *Physica C* **232**, 347 (1994).
- ²⁶F. Zuo, S. Khizroev, G. C. Alexandrakakis, and V. N. Kopylov, *Phys. Rev. B* **52**, R755 (1995).
- ²⁷F. Zuo and V. N. Kopylov, *Physica C* **261**, 289 (1996).
- ²⁸M. Xu, T. W. Li, D. G. Hinks, G. W. Crabtree, H. M. Jaeger, and H. Aoki, *Phys. Rev. B* **59**, 13 632 (1999).
- ²⁹M. Pissas, E. Moraitakis, G. Kallias, A. Terzis, D. Niarchos, and M. Charalambous, *Phys. Rev. B* **58**, 9536 (1998).
- ³⁰G. Ravikumar, V. C. Sahni, P. K. Mishra, T. V. Chandrasekhar Rao, S. S. Banerjee, A. K. Grover, S. Ramakrishnan, S. Bhattaricharya, M. J. Higgins, E. Yamamoto, Y. Haga, M. Hedo, Y. Inada, and Y. Onuki, *Phys. Rev. B* **57**, R11 069 (1998).
- ³¹S. B. Roy and P. Chaddah, *Physica C* **279**, 70 (1997).
- ³²F. Zuo, J. A. Schlueter, U. Geiser, and J. M. Williams, *Phys. Rev. B* **54**, 6107 (1996).
- ³³T. Nishizaki, T. Sasaki, T. Fukase, and N. Kobayashi, *Phys. Rev. B* **54**, R3760 (1996).
- ³⁴W. Harneit, T. Klein, C. Escribe-Filippini, H. Rakoto, J. M. Broto, A. Sulpice, R. Buder, J. Marcus, and W. Shmidbauer, *Physica C* **267**, 270 (1996).
- ³⁵L. Krusin-Elbaum, L. Civale, V. M. Vinokur, and F. Holtzberg, *Phys. Rev. Lett.* **69**, 2280 (1992).
- ³⁶T. Giamarchi and P. Le Doussal, *Phys. Rev. B* **55**, 6577 (1997).
- ³⁷A. E. Koshelev and V. M. Vinokur, *Phys. Rev. B* **57**, 8026 (1998).
- ³⁸V. Vinokur, B. Khaykovich, E. Zeldov, M. Konczykowski, R. A. Doyle, and P. H. Kes, *Physica C* **295**, 209 (1998).
- ³⁹B. Horovitz, *Phys. Rev. B* **60**, R9939 (1999).
- ⁴⁰I. M. Sutjahja, A. A. Nugroho, M. Diantoro, M. O. Tjia, H. Gelders, A. A. Menovsky, and J. J. M. Franse, *Physica C* (to be published).
- ⁴¹L. Burlachkov, V. G. Geshkenbein, A. E. Koshelev, A. I. Larkin, and V. M. Vinokur, *Phys. Rev. B* **50**, 16 770 (1994).
- ⁴²E. Zeldov, A. I. Larkin, V. B. Geshkenbein, M. Konczykowski, D.

- Majer, B. Khaykovich, V. M. Vinokur, and H. Shtrikman, Phys. Rev. Lett. **73**, 1428 (1994).
- ⁴³F. Zuo, D. Vacaru, H. M. Duan, and A. M. Hermann, Phys. Rev. B **47**, 5535 (1993).
- ⁴⁴M. Nideröst, R. Frassanito, M. Saalfrank, A. C. Mota, G. Blatter, V. N. Zavaritsky, T. W. Li, and P. H. Kes, Phys. Rev. Lett. **81**, 3231 (1998).
- ⁴⁵For review, see S. Senoussi, J. Phys. III **2**, 1041 (1992), and references therein.
- ⁴⁶L. I. Glazman and A. E. Koshelev, Phys. Rev. B **43**, 2835 (1991).
- ⁴⁷L. L. Daemen, L. N. Bulaevskii, M. P. Maley, and J. Y. Coulter, Phys. Rev. Lett. **70**, 1167 (1993).
- ⁴⁸G. Blatter, M. Dogdson, and V. Geshkenbein, Physica C **332**, 66 (2000).
- ⁴⁹J. P. Rodriguez, Phys. Rev. B **62**, 9117 (2000).
- ⁵⁰Q. Li, M. Suenaga, T. Kimura, and K. Kishio, Phys. Rev. B **47**, 11 384 (1993).
- ⁵¹Y. Yeshurun and A. P. Malozemoff, Phys. Rev. Lett. **60**, 2202 (1988).
- ⁵²M. Tinkham, Phys. Rev. Lett. **61**, 1658 (1988).
- ⁵³A. Schilling, R. Jin, J. D. Guo, and H. R. Ott, Phys. Rev. Lett. **71**, 1899 (1993).
- ⁵⁴K. Kitazawa, J. Shimoyama, H. Ikuta, T. Sasagawa, and K. Kishio, Physica C **282-287**, 335 (1997).
- ⁵⁵W. Lawrence and S. Doniach, in *Proceedings of the Twelfth International Conference on Low Temperature Physics*, edited by Eizo Kanada (Academic, Kyoto, 1971), p. 361.
- ⁵⁶T. W. Clinton *et al.*, Physica C **235-240**, 1375 (1994).
- ⁵⁷D. Dulic, A. Pimenov, D. van der Marel, D. M. Broun, S. Kamal, W. N. Hardy, A. A. Tsvetkov, I. M. Sutjahja, R. Liang, A. A. Menovsky, A. Loidl, and S. S. Saxena, Phys. Rev. Lett. **86**, 4144 (2001).